ORIGINAL PAPER

Controllability, observability and identifiability in single-phase porous media flow

M. J. Zandvliet · J. F. M. Van Doren · O. H. Bosgra · J. D. Jansen · P. M. J. Van den Hof

Abstract Over the past few years, more and more systems and control concepts have been applied in reservoir engineering, such as optimal control, Kalman filtering, and model reduction. The success of these applications is determined by the controllability, observability, and identifiability properties of the reservoir at hand. The first contribution of this paper is to analyze and interpret the controllability and observability of single-phase flow reservoir models and to investigate how these are affected by well locations, heterogeneity, and fluid properties. The second contribution of this paper is to show how to compute an upper bound on the number of identifiable parameters when history matching production data and to present a new method to regularize the history matching problem using a reservoir's controllability and observability properties.

Keywords Reservoir engineering · Controllability · Observability · Identifiability

Nomenclature

$\mathbf{A}_c, \mathbf{B}_c$	Continuous-time state-space matrices
$\mathbf{A}, \mathbf{B}, \mathbf{C}, \mathbf{D}$	Discrete-time state-space matrices
$\hat{\mathbf{A}}, \hat{\mathbf{B}}, \hat{\mathbf{C}}, \mathbf{D}$	State-space matrices in canonical form
$\tilde{\mathbf{A}}_{11}, \tilde{\mathbf{B}}_1, \tilde{\mathbf{C}}_1, \mathbf{D}$	State-space matrices of controllable and observable part
c	Compressibility
$\mathcal{C}_k$	Controllability matrix
H_∞	Worst case energy norm
J_{con}	Minimal required input energy
J_{obs}	Maximal produced output energy
$\mathbf{J}_p, \mathbf{J}_q$	Matrix of well indices
k_j	Grid block permeability
L	Number of regularized parameters
$\mathbf{L}$	Cholesky factorization of $\mathcal{Q}$
M	Number of uncertain physical parameters
n	Number of time-steps in history matching
N	Total number of grid blocks
$N_{\mathbf{u}}$	Number of manipulated inputs
$N_{\mathbf{y}}$	Number of measured outputs
$N_{\mathbf{y}}$	Maximum number of identifiable parameters
$\mathcal{O}_k$	Observability matrix
$\bar{\mathbf{p}}_1$	Vector of pressures in grid blocks without wells
$\bar{\mathbf{p}}_2$	Vector of pressures in grid blocks with flow-rate controlled wells
$\bar{\mathbf{p}}_3$	Vector of pressures in grid blocks with pressure controlled wells
$\check{\mathbf{p}}_w$	Vector of prescribed pressures
$\bar{\mathbf{p}}_w$	Vector of measured pressures
$\mathbf{p}$	Vector of grid block pressures
$\mathbf{p}_k$	Vector of grid block pressures at time-step k
$\mathbf{p}_r$	Vector of reference pressures

J. D. Jansen (✉)
Faculty of Civil Engineering and Geosciences, Department of Geotechnology, Delft University of Technology,
Stevinweg 1, 2628 CN Delft, The Netherlands
e-mail: j.d.jansen@tudelft.nl

M. J. Zandvliet · J. F. M. Van Doren ·
O. H. Bosgra · P. M. J. Van den Hof
Delft Center for Systems and Control,
Delft University of Technology,
Mekelweg 2, 2628 CD Delft, The Netherlands

$\hat{\mathbf{p}}_k$	Transformed vector of grid block pressures at time-step k
$\mathcal{P}$	Controllability Gramian
$\mathcal{Q}$	Observability Gramian
$\breve{\mathbf{q}}_w$	Vector of prescribed flow rates
$\bar{\mathbf{q}}_w$	Vector of measured flow rates
t	Time
$\hat{\mathbf{t}}_j$	j^{th} column of inverse balancing matrix
$\mathbf{T}$	Transformation matrix
$\mathbf{T}_{\text{bal}}$	Balancing matrix
$\hat{\mathbf{T}}_{\text{bal}}$	Inverse balancing matrix
$\mathbf{T}$	Transmissibility matrix
$\mathbf{u}$	Vector of manipulated inputs
$\mathbf{u}_k$	Vector of manipulated inputs at time-step k
$\mathbf{U}$	Cholesky factorization of $\mathcal{P}$
V	History match cost function
$\mathbf{V}$	Accumulation matrix
$\mathbb{X}^{\text{con}}$	Controllable subspace
$\mathbb{X}^{\text{unobs}}$	Unobservable subspace
$\mathbf{y}$	Vector of measured outputs
$\mathbf{y}_k$	Vector of measured outputs at time-step k
init	Initial
up	Updated
$\boldsymbol{\alpha}$	Vector of regularized parameters
θ_i	Uncertain physical parameter
$\boldsymbol{\theta}$	Vector of uncertain physical parameters
ϵ	Scaling factor
λ	Eigenvalue
λ_{min}	Smallest eigenvalue
μ	Viscosity
σ_k	k^{th} Hankel singular value
σ_{max}	Largest singular value
ϕ_j	Grid block porosity
$\boldsymbol{\Phi}$	Regularization matrix
Δt	Discretization time-step

1 Introduction

Flow though porous media is often modelled by combining a mass-balance equation with Darcy's law, leading to a set of partial differential equations (PDEs). Subsequently, these PDEs are usually discretized in space by dividing the reservoir into a finite number of grid blocks, the properties of which are assumed to be homogeneous. The time-invariant fluid and geological properties of the resulting reservoir model are called the model parameters, whereas the time-varying pressures and saturations in each grid block are called the states. Using an estimate of the model parameters and

an estimate of the initial state, a reservoir simulator computes the state trajectory that results from a certain choice of the well configuration and associated production settings.

Reservoir simulators are, of course, often used to make predictions of future hydrocarbon production. Moreover, reservoir engineers usually try to optimize the predicted output (e.g., in terms of cumulative oil production after 10 years) over the manipulated inputs (e.g. the well configuration and associated production settings). In order to make these predictions more reliable, reservoir engineers often incorporate observations (e.g., measured production rates) into a reservoir model, for example by adapting the estimate of the initial state and the model parameters such that the model predictions match the observations in a history matching procedure. In short, the success of their efforts is essentially determined by the degree to which a reservoir is controllable and observable.

Two fundamental concepts in systems and control theory are controllability and observability. For a linear system, the so-called controllable subspace is defined as the set of states that can be reached by a suitable choice of the control input. Similarly, the unobservable subspace is defined as the set of states that cannot be distinguished from zero through the measured output. Together, these two concepts determine the behavior from controlled input to measured output. Consequently, investigating a linear system's controllability and observability properties is an important step to understanding it. Although the definitions of controllability and observability for nonlinear systems such as oil and gas reservoirs are more complicated, similar reasoning applies. Another important concept in systems and control theory is identifiability. The parameters in a model are said to be identifiable if they can be uniquely estimated from measured output data by a suitable choice of the control input.

Over the past few years, more and more systems and control concepts have been applied in reservoir engineering. Examples include optimal control, Kalman filtering, and model reduction. In these applications, little attention is paid to understanding the controllability, observability, and identifiability properties of the reservoir at hand. This is surprising since, as mentioned earlier, these properties essentially determine a reservoir's behavior and, thereby, the success of the chosen application. Since the concepts of controllability and observability are more complicated for nonlinear systems and since the nonlinearity of oil and gas reservoirs is mainly due to time-varying saturations in multiphase flow, this paper focuses on single-phase flow (Section 2).

The main contributions of this paper are to:

1. Analyze and interpret the controllability and observability of single-phase flow reservoir models and investigate how these are affected by well locations, heterogeneity, and fluid properties (Section 3)
2. Show how to compute an upper bound on the number of identifiable parameters in history matching production data
3. Present a new method to regularize the history matching problem using a reservoir's controllability and observability properties (Section 4)

2 Single-phase flow equations

We consider the usual equations for isothermal weakly compressible single-phase flow through porous media, based on conservation of mass and Darcy's law [4]. Using some form of spatial discretization, such as a finite volume or finite element method, we obtain continuous-time system equations, which can be written in partitioned form as:

$$
\begin{bmatrix} \mathbf{V}_{11} & \mathbf{0} & \mathbf{0} \\ \mathbf{0} & \mathbf{V}_{22} & \mathbf{0} \\ \mathbf{0} & \mathbf{0} & \mathbf{V}_{33} \end{bmatrix} \begin{bmatrix} \dot{\bar{\mathbf{p}}}_1 \\ \dot{\bar{\mathbf{p}}}_2 \\ \dot{\bar{\mathbf{p}}}_3 \end{bmatrix}
$$
$$
+ \begin{bmatrix} \mathbf{T}_{11} & \mathbf{T}_{12} & \mathbf{T}_{13} \\ \mathbf{T}_{21} & \mathbf{T}_{22} & \mathbf{T}_{23} \\ \mathbf{T}_{31} & \mathbf{T}_{32} & \mathbf{T}_{33}+\mathbf{J}_p \end{bmatrix} \begin{bmatrix} \bar{\mathbf{p}}_1 \\ \bar{\mathbf{p}}_2 \\ \bar{\mathbf{p}}_3 \end{bmatrix} = \begin{bmatrix} \mathbf{0} \\ \check{\mathbf{q}}_w \\ \mathbf{J}_p\check{\mathbf{p}}_w \end{bmatrix}, \tag{1}
$$

where the diagonal block matrices, $\mathbf{V}_{ii}$, $i = 1, 2, 3$, are accumulation matrices with entries that depend on the grid block size, grid block porosities, and total compressibility, and the band-diagonal block matrices, $\mathbf{T}_{ij}$, $i = 1, 2, 3$, $j = 1, 2, 3$, are transmissibility matrices with entries that depend on the grid block size, grid block permeabilities, and fluid viscosity. The elements of vector $\mathbf{p}_1$ are the pressures in those grid blocks (elements) that are not penetrated by a well. The elements of $\mathbf{p}_2$ are the pressures in the blocks where the source terms are prescribed well flow rates $\check{\mathbf{q}}_w$, and those of $\mathbf{p}_3$ are the pressures in the blocks where the source terms are obtained through prescription of the bottom hole pressures with the aid of a well inflow model

$$
\bar{\mathbf{q}}_w = \mathbf{J}_p\left(\check{\mathbf{p}}_w - \bar{\mathbf{p}}_3\right), \tag{2}
$$

where $\mathbf{J}_p$ is a diagonal matrix of well indices, the elements of $\check{\mathbf{p}}_w$ are the prescribed pressures, and the elements of $\bar{\mathbf{q}}_w$ are the resulting well flow rates. To compute the bottom hole pressures $\bar{\mathbf{p}}_w$ in the wells where the flow rates have been prescribed, we need an additional diagonal matrix $\mathbf{J}_q$ of well indices such that

$$
\check{\mathbf{q}}_w = \mathbf{J}_q\left(\bar{\mathbf{p}}_w - \bar{\mathbf{p}}_2\right). \tag{3}
$$

Equations 2 and 3 can be combined to give

$$
\begin{bmatrix} \mathbf{0} \\ \bar{\mathbf{p}}_w \\ \bar{\mathbf{q}}_w \end{bmatrix} = \begin{bmatrix} \mathbf{0} & \mathbf{0} & \mathbf{0} \\ \mathbf{0} & \mathbf{I} & \mathbf{0} \\ \mathbf{0} & \mathbf{0} & -\mathbf{J}_p \end{bmatrix} \begin{bmatrix} \bar{\mathbf{p}}_1 \\ \bar{\mathbf{p}}_2 \\ \bar{\mathbf{p}}_3 \end{bmatrix} + \begin{bmatrix} \mathbf{0} & \mathbf{0} & \mathbf{0} \\ \mathbf{0} & \mathbf{J}_q^{-1} & \mathbf{0} \\ \mathbf{0} & \mathbf{0} & \mathbf{J}_p \end{bmatrix} \begin{bmatrix} \mathbf{0} \\ \check{\mathbf{q}}_w \\ \check{\mathbf{p}}_w \end{bmatrix}. \tag{4}
$$

If we define the vectors

$$
\mathbf{p} := \begin{bmatrix} \bar{\mathbf{p}}_1 \\ \bar{\mathbf{p}}_2 \\ \bar{\mathbf{p}}_3 \end{bmatrix} \in \mathbb{R}^N, \quad \mathbf{u} := \begin{bmatrix} \check{\mathbf{q}}_w \\ \check{\mathbf{p}}_w \end{bmatrix} \in \mathbb{R}^{N_\mathbf{u}},
$$

$$
\mathbf{y} := \begin{bmatrix} \bar{\mathbf{p}}_w \\ \bar{\mathbf{q}}_w \end{bmatrix} \in \mathbb{R}^{N_\mathbf{y}},
$$

Equations 1 and 4 can be rewritten as

$$
\dot{\mathbf{p}} = \mathbf{A}_c\mathbf{p} + \mathbf{B}_c\mathbf{u}, \tag{5}
$$

$$
\mathbf{y} = \mathbf{C}\mathbf{p} + \mathbf{D}\mathbf{u}, \tag{6}
$$

where

$$
\mathbf{A}_c = - \begin{bmatrix} \mathbf{V}_{11}^{-1}\mathbf{T}_{11} & \mathbf{V}_{11}^{-1}\mathbf{T}_{12} & \mathbf{V}_{11}^{-1}\mathbf{T}_{13} \\ \mathbf{V}_{22}^{-1}\mathbf{T}_{21} & \mathbf{V}_{22}^{-1}\mathbf{T}_{22} & \mathbf{V}_{22}^{-1}\mathbf{T}_{23} \\ \mathbf{V}_{33}^{-1}\mathbf{T}_{31} & \mathbf{V}_{33}^{-1}\mathbf{T}_{32} & \mathbf{V}_{33}^{-1}\left(\mathbf{T}_{33}+\mathbf{J}_p\right) \end{bmatrix},
$$

$$
\mathbf{B}_c = \begin{bmatrix} \mathbf{0} & \mathbf{0} \\ \mathbf{V}_{22}^{-1} & \mathbf{0} \\ \mathbf{0} & \mathbf{V}_{33}^{-1}\mathbf{J}_p \end{bmatrix}, \quad \mathbf{C} = \begin{bmatrix} \mathbf{0} & \mathbf{I} & \mathbf{0} \\ \mathbf{0} & \mathbf{0} & -\mathbf{J}_p \end{bmatrix},
$$

$$
\mathbf{D} = \begin{bmatrix} \mathbf{J}_q^{-1} & \mathbf{0} \\ \mathbf{0} & \mathbf{J}_p \end{bmatrix}.
$$

Equations 5 and 6 are the standard continuous-time linear time-invariant state space equations as used in the systems and control literature. The matrices $\mathbf{A}_c$, $\mathbf{B}_c$, $\mathbf{C}$, and $\mathbf{D}$ are often referred to as the *system matrix*, the *input matrix*, the *output matrix*, and the *direct throughput matrix*, and the vectors $\mathbf{u}$, $\mathbf{p}$, and $\mathbf{y}$ as the *input vector*, the *state vector*, and the *output vector*, respectively. Using an explicit time discretization, Eqs. 5 and 6 can be rewritten in discrete-time form as

$$
\mathbf{p}_{k+1} = \mathbf{A}\mathbf{p}_k + \mathbf{B}\mathbf{u}_k, \tag{7}
$$

$$
\mathbf{y}_k = \mathbf{C}\mathbf{p}_k + \mathbf{D}\mathbf{u}_k, \tag{8}
$$

where $\mathbf{A} = (\mathbf{I} + \Delta t\mathbf{A}_c)$ and $\mathbf{B} = \Delta t\mathbf{B}_c$. We apply the usual notation $\mathbf{p}_k$ to indicate $\mathbf{p}(k\Delta t)$, where the subscript k is the time step counter or discrete time. The discretization time step is set to

$$
\Delta t = 0.5/\left|\lambda_{\min}\left(\mathbf{A}_c\right)\right|, \tag{9}
$$

where $\lambda_{\min}$ represents the most negative eigenvalue. This leads to quite small time steps and is referred to as the so-called Nyquist–Shannon sampling time needed to accurately capture all of the dynamics in Eq. 5—see [3].

In the following, we show how the controllability and observability of the pressures throughout the reservoir model are determined by the matrix pairs $(\mathbf{A}, \mathbf{B})$ and $(\mathbf{A}, \mathbf{C})$, respectively. We stress, however, that both the theory and results that follow do not depend on implicit or explicit time discretization or on the particular value of the discretization time-step Δt, and also apply to the continuous-time case.

3 Controllability and observability

The material treated in this section was pioneered by [16, 24, 29], and is usually included in any advanced course on systems and control. The reader is referred to these works or, for example, the textbooks [2, 12] for details and proofs.

3.1 Controllability and observability

For a system (Eqs. 7–8) with $N_{\mathbf{u}}$ control inputs (i.e., controlled flow rates or bottom-hole pressures) and $N_{\mathbf{y}}$ outputs (i.e., measured flow rates or bottom-hole pressures), the controllability matrix $\mathcal{C}_k$ and observability matrix $\mathcal{O}_k$ are defined as follows:

$$\mathcal{C}_k(\mathbf{A}, \mathbf{B}) := \begin{bmatrix} \mathbf{B} \ \mathbf{AB} \ \mathbf{A}^2\mathbf{B} \ \ldots \ \mathbf{A}^{k-1}\mathbf{B} \end{bmatrix}, \quad (10)$$

$$\mathcal{O}_k(\mathbf{C}, \mathbf{A}) := \begin{bmatrix} \mathbf{C} \\ \mathbf{CA} \\ \mathbf{CA}^2 \\ \vdots \\ \mathbf{CA}^{k-1} \end{bmatrix}. \quad (11)$$

By the so-called Cayley–Hamilton theorem, the rank of $\mathcal{C}_\infty$ and its image are determined by, at most, the first $N \times N_{\mathbf{u}}$ columns, where N is the state dimension. In other words, $\mathrm{im}(\mathcal{C}_\infty) = \mathrm{im}(\mathcal{C}_N) \subset \mathbb{R}^N$. Similarly, the rank of $\mathcal{O}_\infty$ and its kernel are determined by, at most, the first $N \times N_{\mathbf{y}}$ rows. In other words, $\ker(\mathcal{O}_\infty) = \ker(\mathcal{O}_N) \subset \mathbb{R}^N$.

Given initial condition

$$\mathbf{p}_0 = \bar{\mathbf{p}}_0, \quad (12)$$

it follows from Eqs. 7–8 that

$$\mathbf{p}_n = \mathbf{A}^n \bar{\mathbf{p}}_0 + \sum_{k=0}^{n-1} \mathbf{A}^{n-k-1} \mathbf{B} \mathbf{u}_k. \quad (13)$$

It is clear by inspection of Eq. 13, together with the previous remark on the image of $\mathcal{C}_N$, that $\mathbf{p}_k$ is a linear combination of the columns of $\mathcal{C}_N$, together with a $\mathbf{p}_0$-dependent term. Consequently, if $\mathcal{C}_N$ has full rank, then $\mathrm{im}(\mathcal{C}_N) = \mathbb{R}^N$, and any $\mathbf{p}_N$ can be reached by a

suitable choice of $\{\mathbf{u}_0, \ldots, \mathbf{u}_{N-1}\}$. This is why a linear system of the form Eqs. 7–8 is called controllable[1] if its controllability matrix $\mathcal{C}_N$ has full rank (i.e., rank N). If rank $(\mathcal{C}_N) < N$, then

$$\mathbb{X}^{\mathrm{con}} := \mathrm{im}(\mathcal{C}_N(\mathbf{A}, \mathbf{B})) \subset \mathbb{R}^N \quad (14)$$

is often referred to as the controllable subspace and consists of the states that can be reached by suitable choice of the control.

It is clear by inspection of Eqs. 13 and 8 that $\mathbf{y}_k$ equals $\mathbf{CA}^k \bar{\mathbf{p}}_0$ plus a control-dependent term, which we assume known. Consequently, if $\mathcal{O}_N$ has full rank, then $\ker(\mathcal{O}_N) = \emptyset$ (empty) and any $\bar{\mathbf{p}}_0$ can be distinguished from zero through the measured output $\{\mathbf{y}_0, \ldots, \mathbf{y}_{N-1}\}$. This is why a linear system of the form Eqs. 7–8 is called observable if its observability matrix $\mathcal{O}_N$ has full rank. If rank $(\mathcal{O}_N) < N$, then

$$\mathbb{X}^{\mathrm{unobs}} := \ker(\mathcal{O}_N(\mathbf{C}, \mathbf{A})) \subset \mathbb{R}^N \quad (15)$$

is often referred to as the unobservable subspace and consists of the states that cannot be distinguished from zero through the measured output.

From Eq. 13, it appears that the pressures can become unbounded if $\mathbf{A}$ has an eigenvalue whose magnitude or absolute value is strictly larger than one. It turns out that if at least one well is controlled by its bottom-hole pressure, $\mathbf{A}$ has eigenvalues strictly smaller than one. This is quite intuitive, as increased reservoir pressure through injected water then automatically leads to increased production, which would not be the case if the flow rates of all the other wells are set to zero.

Strictly speaking, all of the states in $\mathbb{X}^{\mathrm{con}}$ can be reached provided that there are no bounds on the manipulated input (i.e., the bottom-hole pressures). Similarly, all of the states not in $\mathbb{X}^{\mathrm{unobs}}$ can, strictly speaking, be distinguished from zero provided that there are no bounds on the accuracy of the measured output (i.e., the flow meters). In practice, neither is realistic. However, there are elements of $\mathbb{X}^{\mathrm{con}}$ that require significantly more energy[2] in terms of

$$\sum_{k=0}^{\infty} \mathbf{u}_k^T \mathbf{u}_k$$

---

[1]Under these conditions, the system is actually called reachable in the systems and control literature, which is equivalent to controllable if $\mathbf{A}$ is nonsingular. Since $\mathbf{A}$ is nonsingular throughout this paper, we stick to the term controllable.

[2]The term "energy" is used loosely here, motivated by the fact that energy can often be written as a quadratic form (e.g., kinetic energy as a function of squared velocity). A more precise term is the squared l_2 norm of the input.

to be reached than others. Similarly, there are elements not in $\mathbb{X}^{\text{unobs}}$ that produce significantly more energy in terms of

$$\sum_{k=0}^{\infty} \mathbf{y}_k^T \mathbf{y}_k$$

when observed than others. To quantify this, the so-called controllability Gramian $\mathcal{P}$ and the observability Gramian $\mathcal{Q}$ are defined as follows:

$$\mathcal{P} := \mathcal{C}_\infty(\mathbf{A}, \mathbf{B}) \mathcal{C}_\infty^T(\mathbf{A}, \mathbf{B}) = \sum_{k=0}^{\infty} \mathbf{A}^k \mathbf{B} \mathbf{B}^T \left(\mathbf{A}^T\right)^k, \quad (16)$$

$$\mathcal{Q} := \mathcal{O}_\infty^T(\mathbf{C}, \mathbf{A}) \mathcal{O}_\infty(\mathbf{C}, \mathbf{A}) = \sum_{k=0}^{\infty} \left(\mathbf{A}^T\right)^k \mathbf{C}^T \mathbf{C} \mathbf{A}^k. \quad (17)$$

These can be computed by solving the so-called discrete-time Lyapunov (or Stein) equations

$$\mathbf{A} \mathcal{P} \mathbf{A}^T + \mathbf{B} \mathbf{B}^T = \mathcal{P}, \quad (18)$$

$$\mathbf{A}^T \mathcal{Q} \mathbf{A} + \mathbf{C}^T \mathbf{C} = \mathcal{Q}, \quad (19)$$

as can be seen by substituting Eqs. 16–17 into Eqs. 18–19 and using the fact that $\mathbf{A}^k \to 0$ for $k \to \infty$ since the eigenvalues of $\mathbf{A}$ are strictly smaller than one. Note that $\text{im}(\mathcal{C}_N) = \text{im}(\mathcal{P})$ and $\ker(\mathcal{O}_N) = \ker(\mathcal{Q})$.

Consider a reference state $\mathbf{p}_r \in \mathbb{R}^N$. In [16], it is shown that the minimal energy J_{con} required to steer the state from $\mathbf{0}$ to $\mathbf{p}_r$ is[3]

$$J_{\text{con}}(\mathbf{p}_r) = \mathbf{p}_r^T \mathcal{P}^{-1} \mathbf{p}_r, \quad (20)$$

and that the maximal energy J_{obs} produced by observing the output of the system whose initial state is given by $\mathbf{p}_r$ is

$$J_{\text{obs}}(\mathbf{p}_r) = \mathbf{p}_r^T \mathcal{Q} \mathbf{p}_r. \quad (21)$$

This means that the elements in $\mathbb{X}^{\text{con}}$ that require the most energy to reach have a significant component in the span of the eigenvectors of $\mathcal{P}$ corresponding to small (absolute) eigenvalues. Similarly, the elements not in $\mathbb{X}^{\text{unobs}}$ that produce the least energy when observed have a significant component in the span of the eigenvectors of $\mathcal{Q}$ corresponding to small (absolute) eigenvalues.

The controllability and observability Gramians, however, are coordinate-dependent, meaning that the energy required/produced to reach/observe reference states depends on the particular choice of coordinates (e.g., the grid block numbering). This can be seen

by considering a linear combination of the original pressures

$$\hat{\mathbf{p}}_k = \mathbf{T} \mathbf{p}_k, \quad (22)$$

with $\mathbf{T} \in \mathbb{R}^{N \times N}$ nonsingular. The dynamics of $\hat{\mathbf{p}}_k$ are given by

$$\hat{\mathbf{p}}_{k+1} = \underbrace{\mathbf{T} \mathbf{A} \mathbf{T}^{-1}}_{=:\tilde{\mathbf{A}}} \hat{\mathbf{p}} + \underbrace{\mathbf{T} \mathbf{B}}_{=:\tilde{\mathbf{B}}} \mathbf{u}_k, \quad (23)$$

$$\mathbf{y}_k = \underbrace{\mathbf{C} \mathbf{T}^{-1}}_{=:\tilde{\mathbf{C}}} \hat{\mathbf{p}}_k + \mathbf{D} \mathbf{u}_k. \quad (24)$$

The associated Gramians $\tilde{\mathcal{P}}$ and $\tilde{\mathcal{Q}}$ satisfy

$$\tilde{\mathcal{P}} = \mathbf{T} \mathcal{P} \mathbf{T}^T, \ \tilde{\mathcal{Q}} = \mathbf{T}^{-T} \mathcal{Q} \mathbf{T}^{-1} \ \Rightarrow \ \tilde{\mathcal{P}} \tilde{\mathcal{Q}} = \mathbf{T} \mathcal{P} \mathcal{Q} \mathbf{T}^{-1}.$$

In other words, by choosing a transformation such that a particular reference state is easier to reach simultaneously makes it harder to observe, and vice versa. Although the Gramians themselves are coordinate-dependent, the eigenvalues of their product are not. The latter are called the Hankel singular values

$$\sigma_k := \sqrt{\lambda_k(\mathcal{P} \mathcal{Q})}, \quad k = 1, \dots, N, \quad (25)$$

and, being coordinate independent, are input–output system invariants.

3.2 Balancing and truncation

We can find a coordinate transformation such that the Gramians $\tilde{\mathcal{P}}$ and $\tilde{\mathcal{Q}}$ are equal, diagonal, and nonnegative. By computing a Cholesky factorization of $\mathcal{P} = \mathbf{U} \mathbf{U}^T$ and $\mathcal{Q} = \mathbf{L} \mathbf{L}^T$ and a singular value decomposition of $\mathbf{U}^T \mathbf{L} = \mathbf{Z} \mathbf{\Sigma} \mathbf{Y}^T$, it can be shown that setting

$$\mathbf{T} = \underbrace{\mathbf{\Sigma}^{-1/2} \mathbf{Y}^T \mathbf{L}^T}_{=:\mathbf{T}_{\text{bal}}} \quad \text{and} \quad \mathbf{T}^{-1} = \underbrace{\mathbf{U} \mathbf{Z} \mathbf{\Sigma}^{-1/2}}_{=:\mathbf{T}_{\text{bal}}^{-1}} \quad (26)$$

leads to

$$\tilde{\mathcal{P}} = \tilde{\mathcal{Q}} = \mathbf{\Sigma} = \text{diag}(\sigma_1, \dots, \sigma_N), \quad (27)$$

where $\sigma_1 \geq \sigma_2 \geq \dots \geq \sigma_N$. $\mathbf{T}_{\text{bal}}$ is called a balancing transformation matrix. Note that because in the balanced coordinates $\tilde{\mathcal{P}} = \tilde{\mathcal{Q}}$, states are equally difficult to reach as observe. In the original coordinates, this means that, letting $\hat{\mathbf{t}}_j$ denote the jth column of $\mathbf{T}_{\text{bal}}^{-1}$, we have

$$J_{\text{con}}(\hat{\mathbf{t}}_j) = 1/\sigma_j \quad \text{and} \quad J_{\text{obs}}(\hat{\mathbf{t}}_j) = \sigma_j.$$

It is important to note that the kth Hankel singular value σ_k can be interpreted as the energy contribution of the kth component of the balanced state $\hat{p}_k$ to the input–output behavior of the system. If the Hankel singular values decrease rapidly, we can therefore conclude that most of the input–output behavior is determined by the first few balanced states. In fact, it can be shown that

---

[3]Assuming $\mathcal{P}^{-1}$ exist, which holds if the system is controllable.

eliminating (or truncating) the last $N - k$ components of the balanced state leads to a reduced k^{th} order approximation of the full N^{th} order system for which the error in input–output behavior, measured in terms of the worst-case energy norm (i.e., the so-called $\mathcal{H}_\infty$ norm), is given by

$$2(\sigma_{k+1} + \ldots + \sigma_N),$$

or twice the sum of the deleted $N - k$ Hankel singular values.

In the following sections, this type of model reduction is not actually applied to reservoir models (as done in [15, 19, 28]). We merely point out that we can analyze when a high-order model in fact behaves like a low-order one. Moreover, we can distinguish between those linear combinations of the pressures that contribute to the input–output behavior and those that do not. In the section that follows, the controllability and observability properties of single-phase flow reservoir models are analyzed and interpreted, and it is shown how these are affected by well locations, heterogeneity, and fluid properties.

3.3 Example 1: homogeneous permeability

Consider a 2D homogeneous reservoir containing one phase and modeled as in the previous section. The model has $21 \times 21 \times 1$ grid blocks of $10\text{m} \times 10\text{m} \times 10\text{m}$. The absolute permeability is 10 mDarcy. The porosity is chosen constant in every grid block and is given by $\phi = 0.20$. The fluid compressibility is $c = 10^{-10}$ Pa^{-1} and viscosity $\mu = 10^{-3}$ Pa s. There are five wells configured in a standard five-spot pattern depicted in Fig. 1. Wells 1, 3, 5, and 4 are production or injection wells. In wells 1, 3, and 5, we can control the bottom-hole pressure; in well 4, the flow rate. Wells 1, 3, 5, and 2 have pressure gauges or flow meters. In wells 1, 3, and 5, we can measure the flow rate; in well 2 (a nonproducing or injecting well), the bottom-hole pressure. The well indices are computed using a Peaceman model with a wellbore radius $r_w = 0.1$ m and skin factor $S = 0$.

The matrices $\mathbf{A}$, $\mathbf{B}$, $\mathbf{C}$, and $\mathbf{D}$ are computed as in Section 2 with a discretization time step given by Eq. 9, which, in this example, leads to $\Delta t = 1.2$ s. In this particular example, the nonzero entries in $\mathbf{C}$ corresponding to the flow rate measurements (i.e., the well indices of wells 1, 3, and 5) are in the order of 10^{-8}: much smaller than the nonzero entry in $\mathbf{C}$ corresponding to the pressure measurement in well 2, which is equal to 1. This is problematic because the previously discussed energy produced by observing pressures in well 2 (in [Pa]^2) will then generally be much larger than the energy produced by observing flow rates in
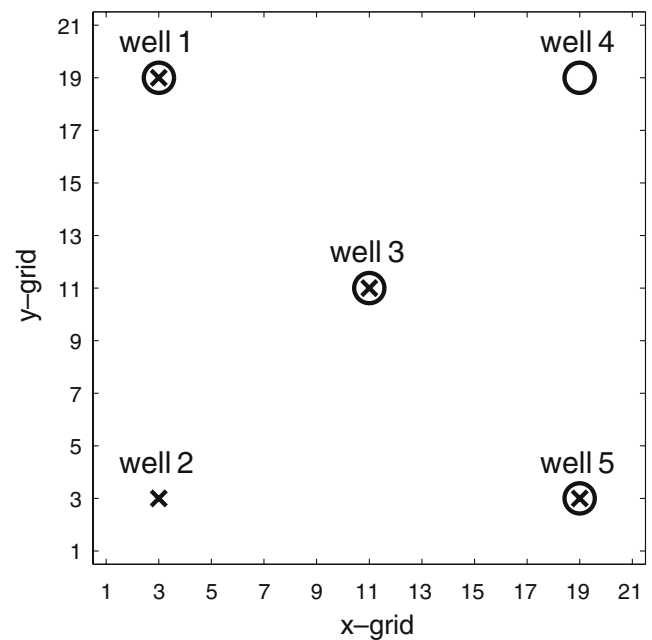

Fig. 1 Well locations: wells 1, 3, and 5 are bottom-hole pressure controlled production or injection wells containing a flow meter (*circled crosses*), well 4 is a flow rate controlled production or injection well without a pressure gauge (*open circle*), and well 2 is an observation well containing a pressure gauge (*cross*)

wells 1, 3, and 5 (in $[\text{m}^3/\text{s}]^2$). In the following examples, the nonzero entry in $\mathbf{C}$ corresponding to the pressure measurement is therefore scaled to the well index of well 2. Similarly, the nonzero entries in $\mathbf{B}$, corresponding to the bottom-hole pressure-controlled wells (i.e., wells 1, 3, and 5), are much smaller than the nonzero entry in $\mathbf{B}$ corresponding to the flow rate controlled well (i.e., well 4). In the following examples, the nonzero entry in $\mathbf{B}$ corresponding to the flow rate controlled well is therefore scaled to the well index of well 4. Subsequently, all of the matrices discussed in the previous section (e.g., Gramians, Hankel singular values, balancing transformation) are computed using the MATLAB functions gram and balreal.

The Hankel singular values, depicted on a logarithmic scale in Fig. 2, decrease very rapidly. This is in line with earlier results from [15, 19, 28] and means that the 441th order reservoir model behaves like a model of much lower order.

The eigenvectors corresponding to the three largest absolute eigenvalues of the Gramians $\mathcal{P}$ and $\mathcal{Q}$, as well as the first three columns of the inverse balancing matrix $\mathbf{T}_{\text{bal}}^{-1}$, are depicted in Fig. 3. In each of the plots, the vector under consideration is projected onto the model grid. Since each component of the state relates to the pressure in a specific grid block, and thereby a specific physical location, this projection allows us to interpret how the reservoir model's controllability and

Fig. 2 All 441 Hankel singular values $\sigma_1, \ldots, \sigma_{441}$ (*left*) and 21 largest ones $\sigma_1, \ldots, \sigma_{21}$ (*right*) for homogeneous example. The *dashed line* represents machine precision
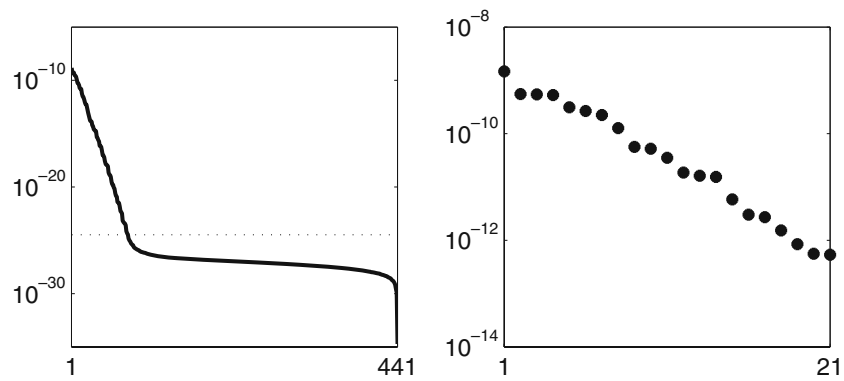

observability properties vary over space. Note that the scales of these plots differ and that the nonzero areas are of particular interest, as these represent areas where reference pressures are controllable and/or observable.

Since the observation well (well 2 in Fig. 1) is the only well that does not appear as a nonzero area in the plots of the controllability Gramian, we conclude that reference pressures in areas near production or injection wells require the least energy to reach. Similarly, since the production well without any measurement (well 4 in Fig. 1) is the only well that does not appear as a nonzero area in the plots of the observability Gramian, we conclude that reference pressures in areas near wells with flow meters or pressure gauges produce the most energy when observed. In short, pressures near wells in which we can control the flow rate or bottom-hole pressure are controllable, whereas pressures near wells in which we can measure the flow rate or bottom-hole pressure are observable. Since a column $\hat{\mathbf{t}}_j$ of the inverse balancing matrix $\mathbf{T}_{\text{bal}}^{-1}$ represents a state (i.e., a vector of pressures) that is equally difficult to reach as observe, it makes sense that particularly the wells in which we can control *and* observe (wells 1, 3 and 5 in Fig. 1) appear as nonzero areas in the plots of $\mathbf{T}_{\text{bal}}^{-1}$.

Remark It is important to mention that the previously mentioned scalings of the entry in **C** corresponding to the pressure measurement in well 2 and entry in **B** corresponding to the flow-rate controlled well 4

Fig. 3 Eigenvectors corresponding to 3 largest absolute eigenvalues of controllability Gramian $\mathcal{P}$ (*top row*), observability Gramian $\mathcal{Q}$ (*middle row*), and first 3 columns of inverse transformation matrix $\mathbf{T}_{\text{bal}}^{-1}$ (*bottom row*) projected onto model grid for homogeneous example
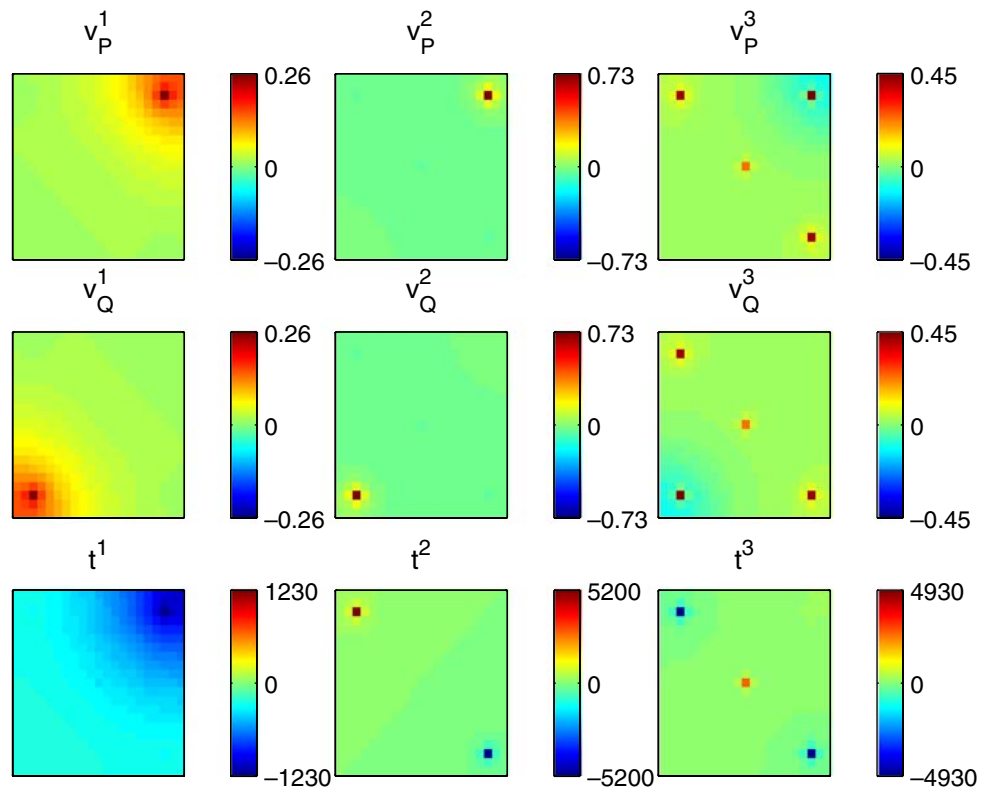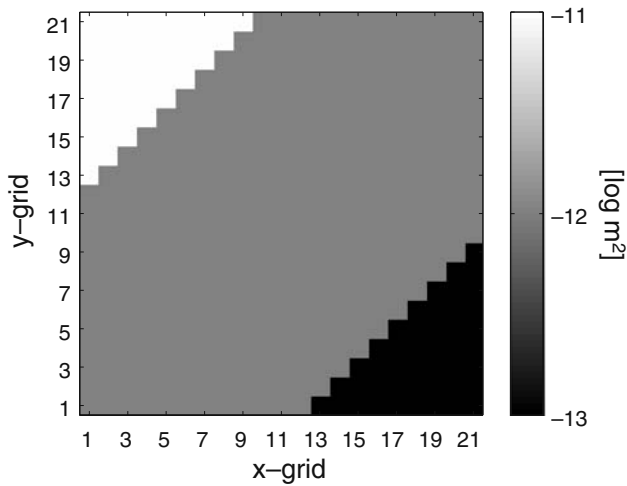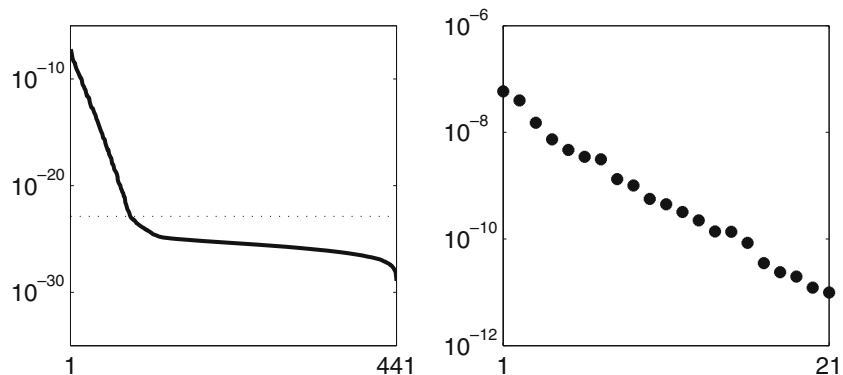
Fig. 4 Heterogeneous permeability

have a large influence on Fig. 3. For example, smaller scaling factors (i.e., smaller entries in **B** and **C**) make the nonzero areas surrounding wells 2 and 4 in Fig. 3 less pronounced. Recall that the main reason for these scalings is that "energy" in $[Pa]^2$ will generally be much larger than in $[m^3/s]^2$. Therefore, if in *each* well, the bottom-hole pressure is controlled and the flow rate is measured (and "required energy" is thereby consistently in $[Pa^2]$ while "produced energy" is consistently in $[m^3/s]^2$), then these scalings are no longer necessary.

3.4 Example 2: heterogeneous permeability

Consider the same reservoir model as in the previous example, but with a high permeability zone of 1,000 mDarcy in the northwest corner, a low permeability zone of 10 mDarcy in the southeast corner, and a permeability of 100 mDarcy throughout the rest of the reservoir—see Fig. 4. The discretization time step Δt is still given by Eq. 9 and its value is therefore different from before, namely, $\Delta t = 0.013$ s.

The results are similar to the homogeneous example. The Hankel singular values, depicted in Fig. 5, decrease very rapidly. As before, this indicates that the 441th-order reservoir model behaves like a model of much lower order.

The eigenvectors corresponding to the three largest absolute eigenvalues of the Gramians $\mathcal{P}$ and $\mathcal{Q}$, as well as the first three columns of $\mathbf{T}_{bal}^{-1}$, are depicted in Fig. 6. Contrary to Fig. 3, only the production well in the high permeable zone (well 1 in Fig. 1) appears as a nonzero area in the plots of the controllability Gramian. From this, we conclude that reference pressures in areas near production wells in high permeable zones require the least energy to reach. Contrary to Fig. 3, only the well with a measurement in the high permeable zone (well 1 Fig. 1) appears as a nonzero area in the plots of the observability Gramian. From this, we conclude that reference pressures in areas near observation wells in high permeable zones produce the most energy when observed. The following section shows how these results depend on the physical reservoir parameters, the time discretization, and the spatial discretization.

3.5 Effect of physical reservoir parameters

Recall that the matrices **A** and **B** in Eq. 7 are given by:

$$\mathbf{A} = I + \mathbf{A}_c \Delta t, \quad \mathbf{B} = \mathbf{B}_c \Delta t.$$
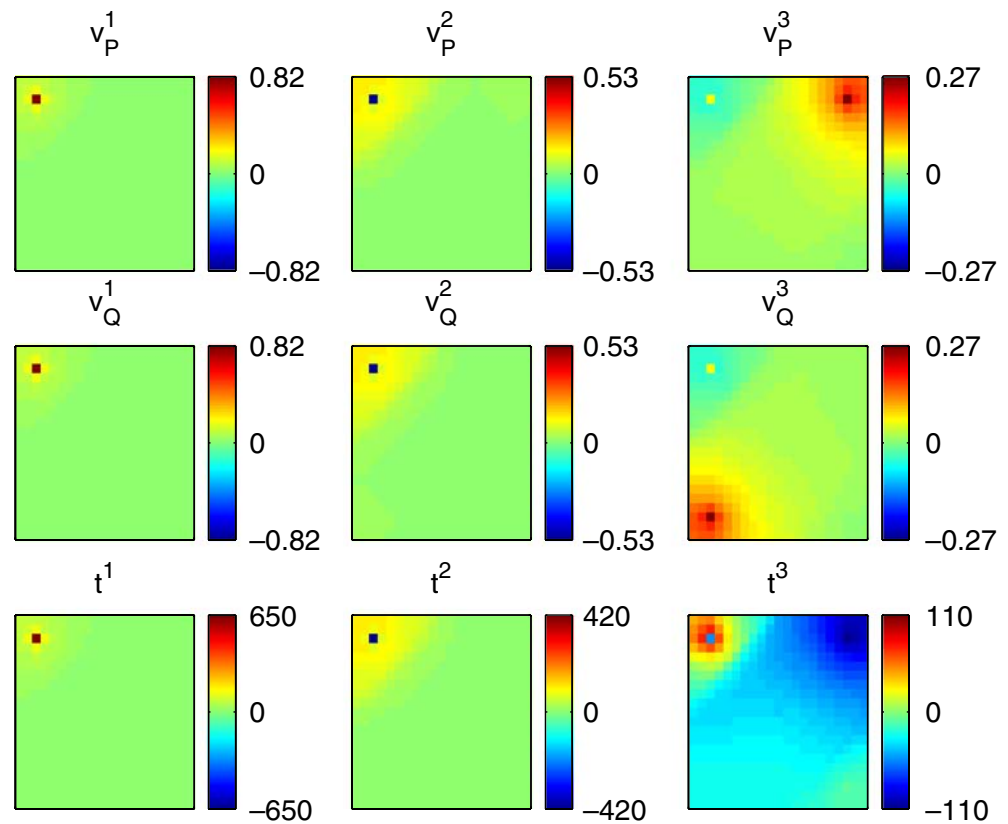
It can be shown that scaling the value of

- compressibility c to $(1/\epsilon)c$, or
- the entire porosity field $\begin{bmatrix} \phi_1 \dots \phi_N \end{bmatrix}$ to $(1/\epsilon) \begin{bmatrix} \phi_1 \dots \phi_N \end{bmatrix}$, or
- viscosity μ to $(1/\epsilon)\mu$, or
- the *entire* permeability field $\begin{bmatrix} k_1 \dots k_N \end{bmatrix}$ to $\epsilon \begin{bmatrix} k_1 \dots k_N \end{bmatrix}$,

for some constant value $\epsilon > 0$ leads to

$$\mathbf{A} = I + \epsilon \mathbf{A}_c \Delta t, \quad \mathbf{B} = \epsilon \mathbf{B}_c \Delta t.$$

Fig. 5 All 441 Hankel singular values $\sigma_1, \dots, \sigma_{441}$ (*left*) and 21 largest ones $\sigma_1, \dots, \sigma_{21}$ (*right*) for heterogeneous example. The *dashed line* represents machine precision

Fig. 6 Eigenvectors corresponding to 3 largest absolute eigenvalues of controllability Gramian $\mathcal{P}$ (*top row*), observability Gramian $\mathcal{Q}$ (*middle row*), and first 3 columns of inverse transformation matrix $\mathbf{T}_{\mathrm{bal}}^{-1}$ (*bottom row*) projected onto model grid for heterogeneous example

In other words, scaling the above mentioned physical parameters by ϵ has the same effect on $\mathbf{A}$ and $\mathbf{B}$ as scaling the discretization time step Δt by ϵ. Furthermore, it can be shown that, for the viscosity or the entire permeability, this also leads to a scaling of the values of $\mathbf{C}$ and $\mathbf{D}$ in Eq. 8 to $\epsilon \mathbf{C}$ and $\epsilon \mathbf{D}$, respectively. Note that in case only certain grid block permeability values are scaled and not the *entire* permeability field, there can be an effect on the controllability and observability properties.

It is important to note that the dynamics of the discrete-time reservoir model Eqs. 7–8 are unaffected by scaling Δt, provided that $\epsilon \Delta t$ is still smaller than the value given by Eq. 9.[4] In fact, the results obtained in this section (in terms of Hankel singular values and spatial variation of controllability and observability properties) using the original continuous-time matrices $(\mathbf{A}_c, \mathbf{B}_c)$ are virtually the same. This therefore also holds for the compressibility and porosity scalings mentioned above. The viscosity and permeability scalings, on the other hand, also influence $\mathbf{C}$, leading to a scaling

of the Hankel singular values $[\sigma_1 \ldots \sigma_N]$ in Eq. 25 to $\epsilon [\sigma_1 \ldots \sigma_N]$.

The spatial discretization also does not have a significant influence on the results: the spatial patterns depicted in Figs. 3 and 6 clearly resemble the ones obtained by modelling the reservoir with, say, $11 \times 11 \times 1$ or $31 \times 31 \times 1$ grid blocks. This is important, as it points out that controllability and observability are reservoir properties, and not just reservoir model properties. Furthermore, the overall decrease in Hankel singular values is very similar—see Fig. 7. This is important, as it points out that the number of grid blocks, often chosen as high as computationally possible, does not have a significant influence on the relevant order of the pressure dynamics throughout the reservoir.

To summarize: the controllability and observability properties of single-phase flow reservoir models have been analyzed, showing that pressures near wells in which we can control the flow rate or bottom-hole pressure are controllable, whereas pressures near wells in which we can measure the flow rate or bottom-hole pressure are observable. These properties are determined by the well configuration and, to a lesser extent, by the heterogeneity of the reservoir at hand. The Hankel singular values of single-phase flow reservoir models decrease rapidly, indicating that they behave as

---

[4]Recall that a discrete-time model Eq. 7 obtained with a time-step larger than Eq. 9 does not capture all of the dynamics of the original continuous-time model Eqs. 5–6.

Fig. 7 All Hankel singular values (*left*) and 21 largest ones (*right*) of three reservoir models based on the reservoir treated in homogenous example, where each model is spatially discretized by a different number of grid blocks
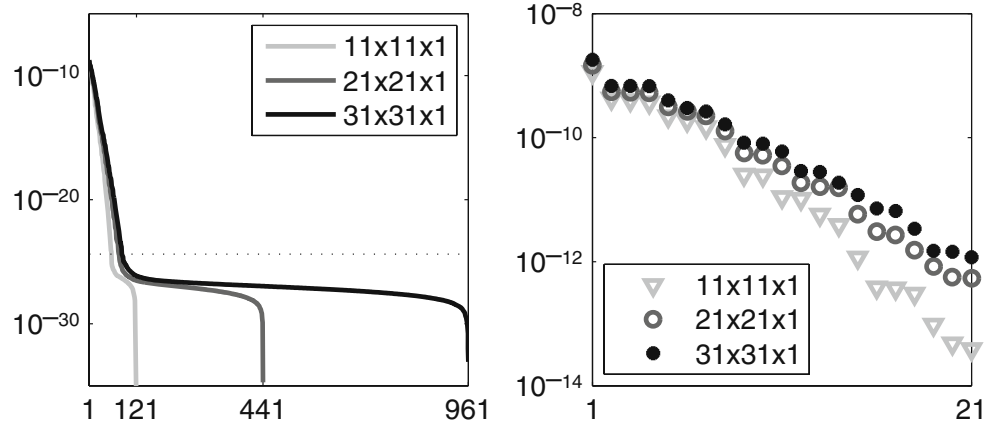
models of much lower order than the order that follows from the number of discretization grid blocks.

Despite these results, there is much work still to be done in this area. Since a reservoir's recovery factor can be defined in terms of the saturations at the end of its lifecycle, a reservoir's saturation dynamics are at least as relevant for field development planning as its pressure dynamics. However, a reservoir's saturation dynamics are described by nonlinear equations, and it is therefore important to investigate how the controllability and observability of saturations change with time. This could be done by linearizing the nonlinear dynamics along a certain trajectory.

4 Identifiability

4.1 History matching and identifiability

Reservoir models generally contain a significant amount of uncertainty originating from many different sources, and this can have a large influence on the predictions of future production. In order to reduce the uncertainty associated with physical reservoir parameters, it is common to define a cost function (typically the weighted squared difference between predicted and measured data), and minimize it over all possible parameter values. In reservoir engineering, this procedure is referred to as history matching, and in this paper, we consider history matching production data to identify physical parameters in single-phase flow reservoirs.

Let us stack all of the uncertain parameters in a vector $\boldsymbol{\theta}$. Furthermore, let us assume that measurements $\bar{\mathbf{y}}_1, \ldots, \bar{\mathbf{y}}_n$ are available, and that these have been generated by the system

$$\mathbf{p}_{k+1} = \mathbf{A}(\boldsymbol{\theta})\mathbf{p}_k + \mathbf{B}(\boldsymbol{\theta})\mathbf{u}_k, \tag{28}$$

$$\mathbf{y}_k = \mathbf{C}(\boldsymbol{\theta})\mathbf{p}_k + \mathbf{D}(\boldsymbol{\theta})\mathbf{u}_k \tag{29}$$

with initial condition

$$\mathbf{p}_0 = \bar{\mathbf{p}}_0 \tag{30}$$

for some unknown $\boldsymbol{\theta} = \bar{\boldsymbol{\theta}}$ (i.e., the parameters of the data-generating system), known manipulated input $\mathbf{u}_0, \ldots, \mathbf{u}_{n-1}$ and known initial state $\bar{\mathbf{p}}_0$, where Eqs. 28 and 29 are the generalizations of Eqs. 7 and 8, respectively. We assume that the input contains enough frequencies to obtain informative measurements, also called persistently exciting—[26]. A common history matching approach is, then, to consider the following nonlinear least-squares problem:

Problem 1

$$\text{minimize} \quad V(\boldsymbol{\theta}) := \sum_{k=1}^{n} \left[\bar{\mathbf{y}}_k - \mathbf{y}_k(\boldsymbol{\theta}) \right]^T \left[\bar{\mathbf{y}}_k - \mathbf{y}_k(\boldsymbol{\theta}) \right],$$

$$\text{over} \quad \boldsymbol{\theta} \in \mathbb{R}^M$$

subject to Eqs. 28, 29, and 30.

Because we assume that all modeling errors are captured in $\boldsymbol{\theta}$ and that the measurements are noisefree, Problem 1 is a least-squares problem with

$$V(\bar{\boldsymbol{\theta}}) = 0, \quad \frac{\partial V}{\partial \boldsymbol{\theta}}(\bar{\boldsymbol{\theta}}) = 0 \quad \text{and} \quad \frac{\partial^2 V}{\partial \boldsymbol{\theta}^2}(\bar{\boldsymbol{\theta}}) \geq 0.$$

If Problem 1 has a unique local minimum at $\boldsymbol{\theta} = \bar{\boldsymbol{\theta}}$ (e.g., $\partial^2 V / \partial \boldsymbol{\theta}^2(\bar{\boldsymbol{\theta}}) > 0$), the model structure (Eqs. 28–29) is said to be locally identifiable. If this minimum is global, the structure is said to be globally identifiable—see [5, 17, 26] for a more detailed discussion.

It is well-known in the petroleum engineering community that if the vector of to-be-estimated physical parameters $\boldsymbol{\theta}$ contains the geological properties (e.g., permeability values) in all grid blocks, virtually all reservoir models of the form Eqs. 28–29 are not identifiable. Often called ill-posed, this lack of identifiability in Problem 1 is mentioned in almost all publications on

history matching and is problematic because a wrongly updated estimate $\boldsymbol{\theta}_{\text{up}}$ of $\bar{\boldsymbol{\theta}}$ can lead to a perfect history match (i.e., $V(\boldsymbol{\theta}_{\text{up}}) = 0$) but incorrect long-term predictions (e.g., when the saturation front has significantly advanced)—see [34].

Since permeability cannot be uniquely estimated from production data, it is common to regularize the problem (i.e., render it "less" ill-posed). The most common method is to add the difference between $\boldsymbol{\theta}$ and the initial estimate $\boldsymbol{\theta}_{\text{init}}$ to the original cost function V

$$V_{\text{reg}}(\boldsymbol{\theta}) := \sum_{k=1}^{n} \left[\bar{\mathbf{y}}_k - \mathbf{y}_k(\boldsymbol{\theta}) \right]^T \mathbf{P_y} \left[\bar{\mathbf{y}}_k - \mathbf{y}_k(\boldsymbol{\theta}) \right]$$
$$+ \left[\boldsymbol{\theta} - \boldsymbol{\theta}_{\text{init}} \right]^T \mathbf{P}_{\boldsymbol{\theta}} \left[\boldsymbol{\theta} - \boldsymbol{\theta}_{\text{init}} \right],$$

where $\mathbf{P_y} \in \mathbb{R}^{N_y}$ and $\mathbf{P}_{\boldsymbol{\theta}} \in \mathbb{R}^N$ are weighting matrices. By weighting the data and prior mismatch terms, the resulting problem can, under certain conditions, be interpreted as finding the maximum a posteriori estimate. This is often referred to as the Bayesian estimation approach to history matching—see [14, 33].

Whatever the history-match cost function V that is considered, it is often minimized using a gradient-based optimization procedure. The gradients $\partial V / \partial \boldsymbol{\theta}$ can be efficiently computed using the so-called adjoint method from optimal control theory—see [10, 11, 20]. The Gauss–Newton and Levenberg–Marquardt methods have been applied, among others, in [25, 30]. A disadvantage of these methods is that they require the sensitivities or partial derivatives of the measurements $\{\mathbf{y}_1, \ldots, \mathbf{y}_n\}$ with respect to the to-be-estimated parameters $\boldsymbol{\theta}$. Despite the use of the adjoint method, this becomes computationally demanding when the number of measurements and the number of parameters are large.

Reducing the computational burden in history matching has been one of the main motivations for reparameterizing $\boldsymbol{\theta}$ by a small number of basis functions (the other being the desire to generate estimates that are geologically realistic). Some of the reparameterization techniques applied in history matching to achieve this include

- Zonation—[20, 23], and adapted versions thereof—[6, 18]
- Grad zones—[7–9]
- Spectral decomposition and subspace methods—[1, 30, 32]
- Kernel principle component analysis—[31]
- Discrete cosine transform—[21, 22]

Despite all of these applications, it is not clear how many parameters can be uniquely identified for any particular reservoir model.

4.2 Number of identifiable parameters

For any k^{th}-order linear system of the form Eqs. 28–29 with $N_{\mathbf{u}}$ manipulated inputs and $N_{\mathbf{y}}$ measured outputs, there exists a transformation $\mathbf{T}_{\text{can}}$ such that, in the transformed coordinates, the state-space matrices that result from Eqs. 23–24 are in a so-called canonical form, which we will denote by

$$\hat{\mathbf{A}}(\boldsymbol{\theta}) := \mathbf{T}_{\text{can}} \mathbf{A}(\boldsymbol{\theta}) \mathbf{T}_{\text{can}}^{-1}, \quad \hat{\mathbf{B}}(\boldsymbol{\theta}) := \mathbf{T}_{\text{can}} \mathbf{B}(\boldsymbol{\theta}),$$
$$\hat{\mathbf{C}} := \mathbf{C}(\boldsymbol{\theta}) \mathbf{T}_{\text{can}}^{-1}, \quad \mathbf{D}(\boldsymbol{\theta}).$$

There are several canonical forms for linear multivariable systems. We consider the one discussed in [13, 26, 27], which has the following form:

- $\hat{\mathbf{A}}$ is initially filled with zeros and ones along the superdiagonal. The $N_{\mathbf{y}}$ rows $r_1, r_2, r_{N_{\mathbf{y}}}$, where $r_0 = 0$ and $r_{N_{\mathbf{y}}} = k$, are filled with parameters.
- $\hat{\mathbf{B}}$ is filled with parameters.
- $\hat{\mathbf{C}}$ is filled with zeros, but each row i has a one in column $r_{i-1} + 1$.

The parameterization is uniquely characterized by the $N_{\mathbf{y}}$ numbers r_i that are to be chosen by the user. Note that only $N_{\mathbf{y}}$ rows in $\hat{\mathbf{A}}$ have elements not equal to zero or one, $\hat{\mathbf{B}}$ is a full matrix and $\hat{\mathbf{C}}$ only contains zeros and ones.

As an example, for the specific situation that $k = 9$, $N_{\mathbf{u}} = 2$, $N_{\mathbf{y}} = 3$, $r_1 = 3$, $r_2 = 5$, and $r_3 = 9$ this canonical form is as follows:

$$\hat{\mathbf{A}}(\boldsymbol{\theta}) = \begin{bmatrix} 0 & 1 & 0 & 0 & 0 & 0 & 0 & 0 & 0 \\ 0 & 0 & 1 & 0 & 0 & 0 & 0 & 0 & 0 \\ \times & \times & \times & \times & \times & \times & \times & \times & \times \\ 0 & 0 & 0 & 0 & 1 & 0 & 0 & 0 & 0 \\ \times & \times & \times & \times & \times & \times & \times & \times & \times \\ 0 & 0 & 0 & 0 & 0 & 0 & 1 & 0 & 0 \\ 0 & 0 & 0 & 0 & 0 & 0 & 0 & 1 & 0 \\ 0 & 0 & 0 & 0 & 0 & 0 & 0 & 0 & 1 \\ \times & \times & \times & \times & \times & \times & \times & \times & \times \end{bmatrix}, \quad \hat{\mathbf{B}}(\boldsymbol{\theta}) = \begin{bmatrix} \times & \times \\ \times & \times \\ \times & \times \\ \times & \times \\ \times & \times \\ \times & \times \\ \times & \times \\ \times & \times \\ \times & \times \end{bmatrix},$$

$$\hat{\mathbf{C}} = \begin{bmatrix} 1 & 0 & 0 & 0 & 0 & 0 & 0 & 0 & 0 \\ 0 & 0 & 0 & 1 & 0 & 0 & 0 & 0 & 0 \\ 0 & 0 & 0 & 0 & 0 & 1 & 0 & 0 & 0 \end{bmatrix}, \quad \mathbf{D}(\boldsymbol{\theta}) = \begin{bmatrix} \times & \times \\ \times & \times \\ \times & \times \end{bmatrix},$$

and, as such, is completely described by the nonzero elements of $\hat{\mathbf{A}}$, $\hat{\mathbf{B}}$, and $\mathbf{D}$. In other words, any k^{th}-order linear system of the form Eqs. 28–29 with $N_{\mathbf{u}}$ manipulated inputs and $N_{\mathbf{y}}$ can be completely described by at most

$$N_{\max} = (N_{\mathbf{u}} + N_{\mathbf{y}}) \times k + N_{\mathbf{u}} N_{\mathbf{y}} \tag{31}$$

parameters—[26]. In the example above, $N_{\max} = 51$.

However, as shown in Section 3, the relevant order k of single-phase flow reservoir models is much smaller than their original order N (determined by the number of grid blocks, often chosen as high as possible). Furthermore, while the physical reservoir parameters (e.g., the grid block permeabilities) do influence the input–output behavior, they do not significantly influence the relevant *order* of the input–output behavior (e.g., Figs. 2 and 5 show the same rapid decline in Hankel singular values). This means that, unless there are many wells $N_{\mathbf{u}}$ in which we can control the flow rate or bottom-hole pressure and many wells $N_{\mathbf{y}}$ in which we can observe the flow rate or bottom-hole pressure, the number of identifiable parameters will be much smaller than the number of grid blocks N. Consequently, if the grid block permeabilities are to be estimated, the resulting reservoir model structure is not identifiable. We stress that this lack of identifiability is not the result of applying a particular transformation to the original state-space matrices $\{\mathbf{A}(\boldsymbol{\theta}), \mathbf{B}(\boldsymbol{\theta}), \mathbf{C}(\boldsymbol{\theta}), \mathbf{D}(\boldsymbol{\theta})\}$ describing single-phase flow, but that there are fundamental reasons for it.

For example, consider again the homogeneous single-phase flow reservoir model of Section 3.3. Recall that the reservoir is modeled by $21 \times 21 \times 1$ grid blocks, and the order of the model is, therefore, $N = 441$. However, the Hankel singular values depicted in Fig. 2 decline very rapidly. In fact, we have

$$2(\sigma_{16} + \ldots + \sigma_{441}) = 8.0 \times 10^{-3}.$$

According to Section 3, the H_∞ norm of the error between the full order model and a 15th-order approximation is therefore less than 10^{-2}. In other words, the relevant order of the model is $k = 15$ and the relevant input–output behavior is described by at most

$$N_{\max} = (N_{\mathbf{u}} + N_{\mathbf{y}}) \times k + N_{\mathbf{u}} N_{\mathbf{y}}$$
$$= (4 + 4) \times 15 + 4 \times 4 = 136$$

parameters. If $\boldsymbol{\theta}$ contains the permeability in all 441 grid blocks, then the model structure Eqs. 28–29 is clearly not identifiable. This gap between the maximum number of identifiable parameters $N_{\max}$ and the number of to-be-identified parameters (e.g., N in the case of grid block permeabilities) is much larger for realistic reservoir models with $N = 10^4 - 10^6$ grid blocks.

4.3 Relevant spatial patterns of permeability

In Section 3, it was demonstrated that Eqs. 28–29 can be decomposed into a part that is both controllable and observable (i.e., belongs to the k largest Hankel singular values) and a part that is poorly controllable and/or poorly observable (i.e., belongs to the $N - k$ smallest Hankel singular values). The choice of k of course depends on what is considered to be relevant for the input–output behavior. For example, if the H_∞ norm of the approximation error should be less than 10^{-3}, k will generally be larger than for 10^{-2}. Let us assume that a particular choice for k has been made, and let $\mathbf{T}_{\mathrm{bal}}$ denote the balancing matrix as introduced in Section 3.2, corresponding to Eqs. 28–29. The controllable and observable part of Eqs. 28–29 is represented by

$$\{\tilde{\mathbf{A}}_{11}(\boldsymbol{\theta}), \tilde{\mathbf{B}}_1(\boldsymbol{\theta}), \tilde{\mathbf{C}}_1(\boldsymbol{\theta}), \mathbf{D}(\boldsymbol{\theta})\},$$

resulting from

$$\begin{bmatrix} \mathbf{T}_{\mathrm{bal},1} & \mathbf{0} \\ \mathbf{T}_{\mathrm{bal},2} & \mathbf{0} \\ \hline \mathbf{0} & \mathbf{I} \end{bmatrix} \begin{bmatrix} \mathbf{A}(\boldsymbol{\theta}) & \mathbf{B}(\boldsymbol{\theta}) \\ \hline \mathbf{C}(\boldsymbol{\theta}) & \mathbf{D}(\boldsymbol{\theta}) \end{bmatrix} \begin{bmatrix} \hat{\mathbf{T}}_{\mathrm{bal},1} & \hat{\mathbf{T}}_{\mathrm{bal},2} & \mathbf{0} \\ \mathbf{0} & \mathbf{0} & \mathbf{I} \end{bmatrix}$$
$$= \begin{bmatrix} \tilde{\mathbf{A}}_{11}(\boldsymbol{\theta}) & \tilde{\mathbf{A}}_{12}(\boldsymbol{\theta}) & \tilde{\mathbf{B}}_1(\boldsymbol{\theta}) \\ \tilde{\mathbf{A}}_{21}(\boldsymbol{\theta}) & \tilde{\mathbf{A}}_{22}(\boldsymbol{\theta}) & \tilde{\mathbf{B}}_2(\boldsymbol{\theta}) \\ \hline \tilde{\mathbf{C}}_1(\boldsymbol{\theta}) & \tilde{\mathbf{C}}_2(\boldsymbol{\theta}) & \mathbf{D}(\boldsymbol{\theta}) \end{bmatrix},$$

where $\tilde{\mathbf{A}}_{12}(\boldsymbol{\theta})$, $\tilde{\mathbf{A}}_{21}(\boldsymbol{\theta})\tilde{\mathbf{B}}_2(\boldsymbol{\theta})$, and $\tilde{\mathbf{C}}_2(\boldsymbol{\theta})$ are almost zero and $\mathbf{T}_{\mathrm{bal}}$ and $\mathbf{T}_{\mathrm{bal}}^{-1}$ have been partitioned according to the first k rows and columns, respectively:

$$\mathbf{T}_{\mathrm{bal}} = \begin{bmatrix} \mathbf{T}_{\mathrm{bal},1} \\ \mathbf{T}_{\mathrm{bal},2} \end{bmatrix} \quad , \quad \mathbf{T}_{\mathrm{bal}}^{-1} = \begin{bmatrix} \hat{\mathbf{T}}_{\mathrm{bal},1} & \hat{\mathbf{T}}_{\mathrm{bal},2} \end{bmatrix}.$$

This decomposition is depicted in Fig. 8.

From a history-matching perspective, it clearly only makes sense to change an initial permeability estimate $\boldsymbol{\theta}$ in a direction $\Delta\boldsymbol{\theta}$ that affects the cost function V as defined in Problem 1. Similarly, from a controllability and observability perspective, it clearly only makes sense to change an initial permeability estimate in a direction that affects the controllable and observable part of the reservoir model (i.e., the quadruple $\{\tilde{\mathbf{A}}_{11}(\boldsymbol{\theta}), \tilde{\mathbf{B}}_1(\boldsymbol{\theta}), \tilde{\mathbf{C}}_1(\boldsymbol{\theta}), \mathbf{D}(\boldsymbol{\theta})\}$ in Fig. 8). If the inputs are persistently exciting, this boils down to the same thing.

Consider the special situation that $\boldsymbol{\theta}$ contains the permeability values in all N grid blocks, or

$$\boldsymbol{\theta} = \begin{bmatrix} k_1 & \ldots & k_N \end{bmatrix}^T. \tag{32}$$

Let us focus on the effect of a variation $\Delta\boldsymbol{\theta}$ on $\{\tilde{\mathbf{A}}_{11}(\boldsymbol{\theta}), \tilde{\mathbf{B}}_1(\boldsymbol{\theta}), \tilde{\mathbf{C}}_1(\boldsymbol{\theta}), \mathbf{D}(\boldsymbol{\theta})\}$ in the coordinates corresponding to a fixed $\mathbf{T}_{\mathrm{bal}}$. Recall from Section 2 that

Fig. 8 Decomposition of a reservoir model into a controllable and observable part, and a poorly controllable and poorly observable part that hardly contributes to the input–output behavior (the *double slash* signs indicate poor coupling)
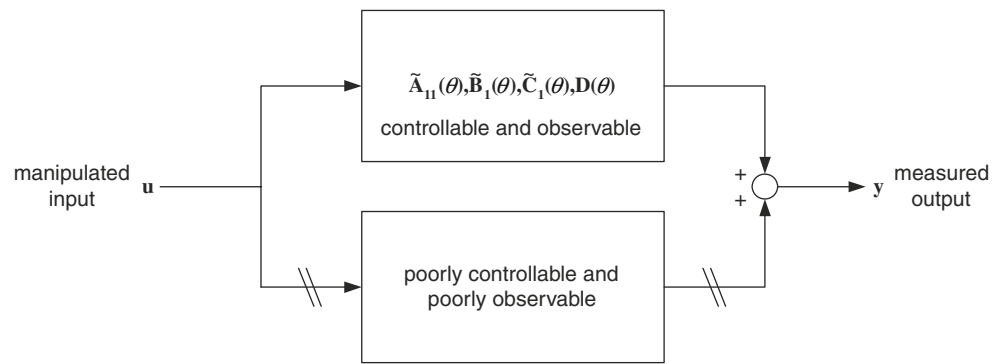
the permeability value k_j only enters **B** if grid block j contains a well. A variation $\Delta\theta_j$ will therefore only have an effect on $\tilde{\mathbf{B}}_1$ if grid block j contains a well. The same reasoning applies to $\tilde{\mathbf{C}}_1$ and **D**. On the other hand, the effect of a variation $\Delta\boldsymbol{\theta}$ on $\tilde{\mathbf{A}}_{11}$ is

$$
\mathbf{T}_{\text{bal},1}\mathbf{A}(\boldsymbol{\theta}+\Delta\boldsymbol{\theta})\hat{\mathbf{T}}_{\text{bal},1} - \underbrace{\mathbf{T}_{\text{bal},1}\mathbf{A}(\boldsymbol{\theta})\hat{\mathbf{T}}_{\text{bal},1}}_{=\tilde{\mathbf{A}}_{11}(\boldsymbol{\theta})}
$$

$$
= \sum_{j=1}^{N}\mathbf{T}_{\text{bal},1}\frac{\partial\mathbf{A}}{\partial\theta_j}(\boldsymbol{\theta})\hat{\mathbf{T}}_{\text{bal},1}\Delta\theta_j + o(\Delta\boldsymbol{\theta}). \tag{33}
$$

where o denotes terms of small order $\Delta\boldsymbol{\theta}$. By defining $\Pi(\boldsymbol{\theta})\in\mathbb{R}^{k^2\times N}$

$$
\Pi(\boldsymbol{\theta}) := \left[\text{vec}\left\{\mathbf{T}_{\text{bal},1}\frac{\partial\mathbf{A}}{\partial\theta_1}(\boldsymbol{\theta})\hat{\mathbf{T}}_{\text{bal},1}\right\}\cdots\right.
$$

$$
\left.\text{vec}\left\{\mathbf{T}_{\text{bal},1}\frac{\partial\mathbf{A}}{\partial\theta_N}(\boldsymbol{\theta})\hat{\mathbf{T}}_{\text{bal},1}\right\}\right], \tag{34}
$$

we can rewrite Eq. 33 as

$$
\text{vec}\left\{\mathbf{T}_{\text{bal},1}\mathbf{A}(\boldsymbol{\theta}+\Delta\boldsymbol{\theta})\hat{\mathbf{T}}_{\text{bal},1} - \underbrace{\mathbf{T}_{\text{bal},1}\mathbf{A}(\boldsymbol{\theta})\hat{\mathbf{T}}_{\text{bal},1}}_{=\tilde{\mathbf{A}}_{11}(\boldsymbol{\theta})}\right\}
$$

$$
= \Pi(\boldsymbol{\theta})\Delta\boldsymbol{\theta} + o(\Delta\boldsymbol{\theta}). \tag{35}
$$

Consider again the homogeneous example of Section 3.3. In Section 4.2, we computed that the relevant order of the model is $k = 15$. The matrix Π can now be computed using Eq. 34. The right singular vectors corresponding to the three largest singular values of Π are depicted in Fig. 9. In each of the plots, the vector under consideration is projected onto the model grid. Since each component of $\boldsymbol{\theta}$ relates to the permeability k_j in a specific grid block j and, thereby, a specific physical location, this projection allows us to interpret how the reservoir model's relevant input–output behavior (as captured by $\tilde{\mathbf{A}}_{11}$) varies over space. Note that the scales of these plots differ and that the nonzero areas are of particular interest, as these represent areas where changes in permeability affect the input–output behavior.

Since wells 2 and 4 from Fig. 1 do not appear as nonzero areas in the plots of Fig. 9, we conclude that permeability variations in grid blocks near wells in which we can both control and observe affect the input–output behavior more than permeability variations in grid blocks far from these wells. This is in line with results presented in [35], and is also very similar to the results from Section 3 on how a reservoir model's controllability and observability properties vary over space. In fact, the nonzero areas in the plots of Fig. 9 strongly resemble those in the bottom row of Fig. 3. In

Fig. 9 Right singular vectors corresponding to three largest singular values of Π projected onto model grid for homogeneous example

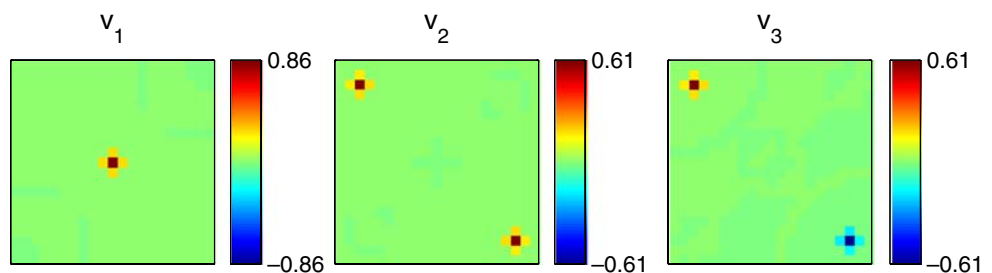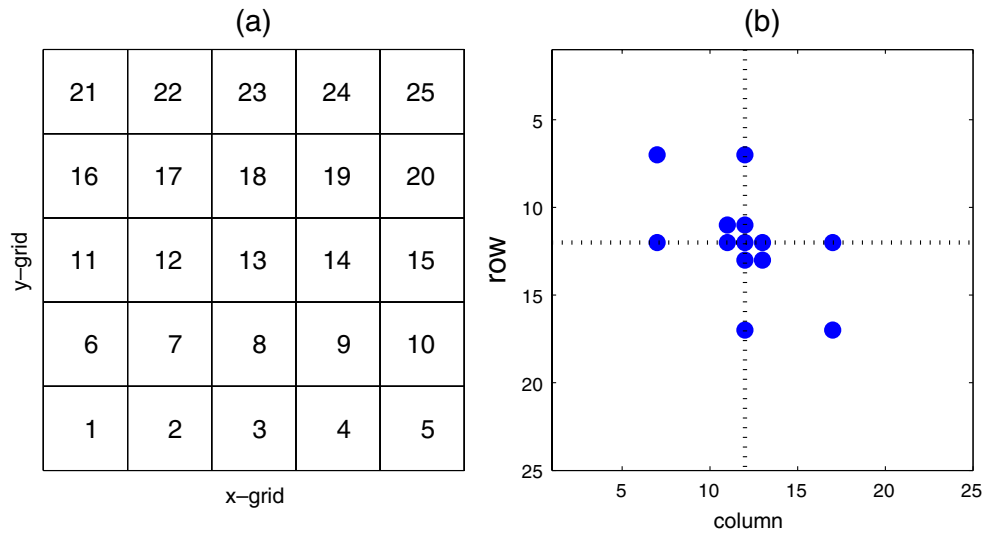**Fig. 10** Grid block numbering for a 2D model of 5×5 grid blocks (**a**) and corresponding nonzero elements of $\partial \mathbf{A}/\partial \theta_{12}$ (**b**). Note that these only appear in the rows and columns of grid block 12 and its neighbors 7, 11, 13, and 17

other words, the relevant spatial patterns of pressure strongly resemble the relevant spatial patterns of permeability. This can be explained as follows.

The matrices $\mathbf{T}_{ij}$ from Section 2, which are used to construct $\mathbf{A}$, have a very sparse structure. Consequently, $\mathbf{A}$ also has a very sparse structure, as does $\partial \mathbf{A}/\partial \boldsymbol{\theta}_j$. In fact, $\partial \mathbf{A}/\partial \boldsymbol{\theta}_j$ has, at most, 13 nonzero elements for a 2D reservoir model—see Fig. 10. Moreover, the nonzero components of $\partial \mathbf{A}/\partial \boldsymbol{\theta}_j$ only appear in the rows and columns corresponding to grid block j and its neighbors.

Similarly, Figs. 3 and 6 show that the nonzero components of $\hat{\mathbf{T}}_{\mathrm{bal},1}$ spatially correspond to grid blocks near wells in which we can both control and observe. Although not depicted in any of the figures, this also holds for the rows of $\mathbf{T}_{\mathrm{bal},1}$. Consequently, the

$$\mathbf{T}_{\mathrm{bal},1} \frac{\partial \mathbf{A}}{\partial \theta_j}(\boldsymbol{\theta}) \hat{\mathbf{T}}_{\mathrm{bal},1}$$

term in Eq. 33 and thereby the jth column of Π only contains nonzero elements if j corresponds to a grid block near a production or injection well with a flow meter or a pressure gauge.

To summarize: the relevant spatial patterns of permeability strongly resemble the relevant spatial patterns of pressure. This is quite intuitive, as it implies

that permeability in an area where we can control and observe has a greater effect on the input–output behavior than in an area where we cannot.

4.4 Controllability and observability-based reparameterization

In Section 4.2, it was shown that the model structure of Eqs. 28–29 is not identifiable if $\boldsymbol{\theta}$ contains the grid block permeability values as in Eq. 32. We therefore propose to regularize Problem 1 by reparameterizing $\boldsymbol{\theta}$ as

$$\boldsymbol{\theta} = \boldsymbol{\Phi}\boldsymbol{\alpha}, \qquad (36)$$

where $\boldsymbol{\Phi} \in \mathbb{R}^{N \times L}$ is called the reparameterization matrix and $L \ll N$ is the number of to-be-estimated (non-physical) parameters (i.e., the number of elements in $\boldsymbol{\alpha}$). The columns of $\boldsymbol{\Phi}$ are referred to as basis functions, and linear combinations of these can represent relevant spatial patterns of permeability.

Since the relevant spatial patterns of permeability strongly resemble the relevant spatial patterns of pressure, we propose to choose the first $L-1$ columns of the inverse balancing matrix $\hat{\mathbf{T}}_{\mathrm{bal},1}$, with an additional vector of ones to account for an overall increase or decrease in permeability. By solving the regularized problem

Fig. 11 Iterative procedure for controllability and observability-based reparameterization of grid block permeabilities
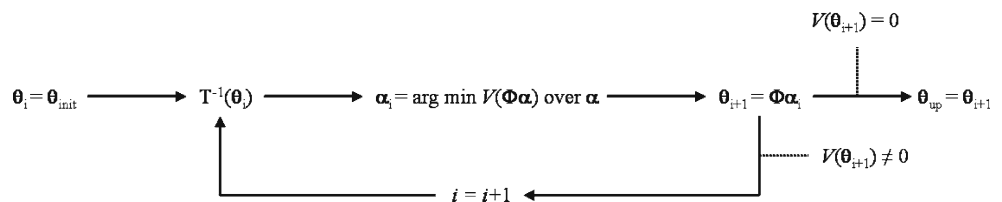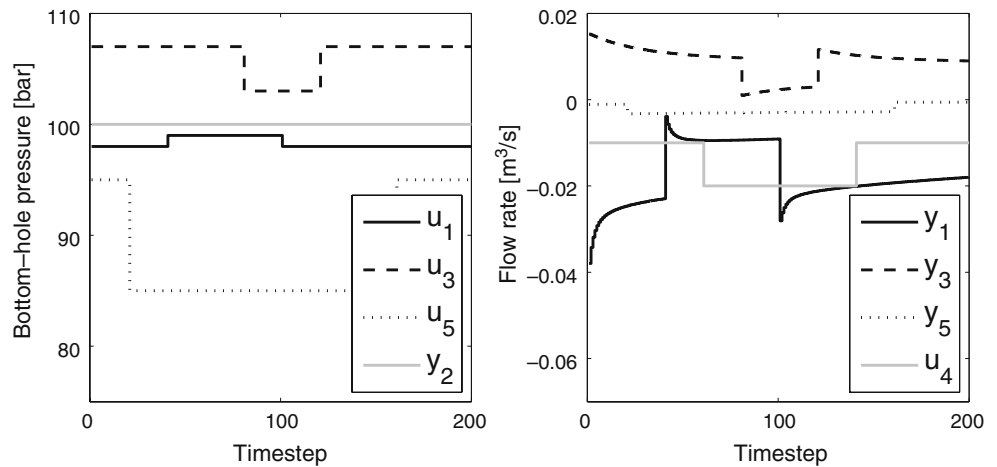
Fig. 12 Bottom-hole pressures (*left*) and flow rates (*right*)

Problem 2

$$\text{minimize} \quad V(\boldsymbol{\Phi\alpha}) = \sum_{k=1}^{n} \left[\bar{\mathbf{y}}_k - \mathbf{y}_k(\boldsymbol{\Phi\alpha}) \right]^T \left[\bar{\mathbf{y}}_k - \mathbf{y}_k(\boldsymbol{\Phi\alpha}) \right]$$

$$\text{over} \qquad \boldsymbol{\alpha} \in \mathbb{R}^L$$

$$\text{subject to} \quad \mathbf{p}_{k+1} = \mathbf{A}(\boldsymbol{\Phi\alpha})\mathbf{p}_k + \mathbf{B}(\boldsymbol{\Phi\alpha})\mathbf{u}_k,$$

$$\mathbf{p}_0 = \bar{\mathbf{p}}_0,$$

$$\mathbf{y}_k = \mathbf{C}(\boldsymbol{\Phi\alpha})\mathbf{p}_k + \mathbf{D}(\boldsymbol{\Phi\alpha})\mathbf{u}_k.$$

using a gradient-based optimization procedure starting from an initial estimate $\boldsymbol{\theta}_{\text{init}} = \boldsymbol{\Phi\alpha}_{\text{init}}$, we only update the permeability in directions that affect the controllable and observable part of the reservoir model and, thereby, V. Note that L should be smaller than or equal to $N_{\max}$, as given by Eq. 31, if Problem 2 is to have a unique solution.

However, $\hat{\mathbf{T}}_{\text{bal},1}$ varies with $\boldsymbol{\theta}$—see, for example, the lower plots in Fig. 3, which closely resemble but are not identical to those in Fig. 6. Therefore, our approach might lead to a local minimum for Problem 2 that is not equal to zero (i.e., not a perfect history match). An alternative method is therefore depicted in Fig. 11. Here, $\hat{\mathbf{T}}_{\text{bal},1}$ is reevaluated if there is no more decrease in V and a local minimum for Problem 2 is found. This reevaluation leads to a new set of basis functions, which might possibly succeed in further decreasing V. This controllability and observability-based regularization is applied in the following example.

4.5 Example

Consider again the heterogeneous reservoir treated in Section 3 and the problem of identifying the logarithm[5] of its permeability as depicted in Fig. 4. This permeability, whose logarithm is denoted by $\bar{\boldsymbol{\theta}}$, is assumed to be the only source of uncertainty. There are 200 perfect pressure measurements $\bar{\mathbf{y}}_1, \ldots, \bar{\mathbf{y}}_{200}$ available every $\Delta t = 0.013$ s, which have been generated by Eqs. 28–29 using $\boldsymbol{\theta} = \bar{\boldsymbol{\theta}}$, an initial state of $\mathbf{p}_0 = 100$ bar, and a manipulated input $\mathbf{u}_0, \ldots, \mathbf{u}_{199}$ depicted in Fig. 12. This input contains enough frequencies to obtain informative measurements (i.e., it is persistently exciting).
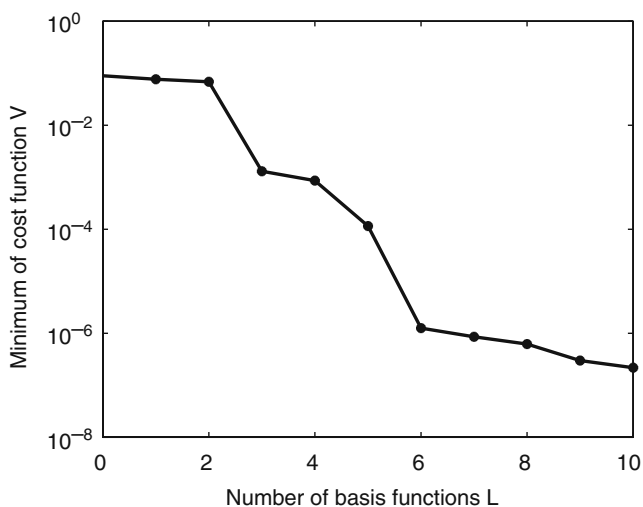

Fig. 13 Minimum value of history match cost function V for different number of basis functions L

---

[5]The logarithm of permeability is used in order to avoid negative permeability estimates and to improve the numerical conditioning of the problem.
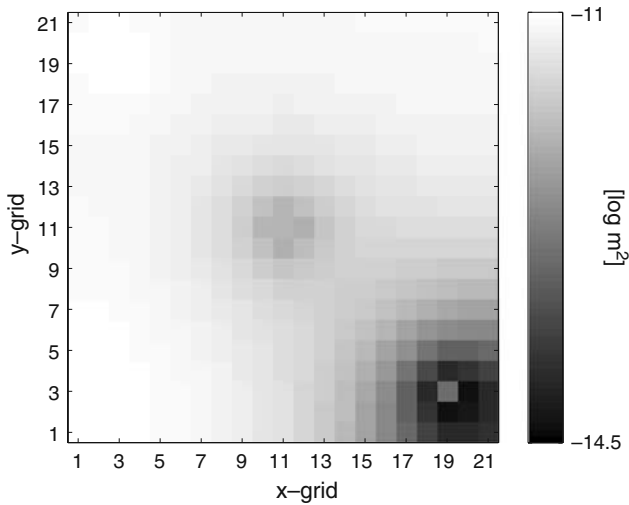
Fig. 14 Updated estimate of heterogeneous permeability using 4 basis functions

The initial estimate θ_{init} of $\bar{\theta}$ is chosen to be homogeneous with a permeability equivalent to 5 mD $= 5 \times 10^{-14}$ m^2. Since we estimate the logarithm of permeability in square meters, the initial estimate is $^{10}\log(5 \times 10^{-14}) = -13.3$. Based on this estimate, the Hankel singular values and the balancing matrix $\mathbf{T}_{\text{bal}}(\theta_{\text{init}})$ are computed as in Section 3 using $\Delta t = 0.013$ s. We stress that this balancing matrix corresponds to the initially estimated model, and not the true one. The squared difference of the measured outputs of this model with the true measured outputs, as defined in Eq. 37, is $V(\theta_{\text{init}}) = 8.7 \times 10^{-2}$. The goal is to update this estimate by solving Problem 2 using a gradient-based optimization procedure (e.g., the MATLAB function lsqnonlin).

The reparameterization matrix $\mathbf{\Phi}$ is chosen as

$$\mathbf{\Phi} = \begin{bmatrix} \mathbf{I}_{N \times 1} & \hat{\mathbf{t}}_1 & \dots & \hat{\mathbf{t}}_L \end{bmatrix}, \tag{37}$$

$$\boldsymbol{\alpha}_{\text{init}} = \begin{bmatrix} -13.3 & 0 & \dots & 0 \end{bmatrix}. \tag{38}$$

where $\hat{\mathbf{t}}_j$ denotes the jth column of $\mathbf{T}_{\text{bal}}^{-1}$. The number of columns L of the reparameterization matrix $\mathbf{\Phi}$ should be smaller or equal to the maximum number of identifiable parameters, which, in this case, is $N_{\text{max}} = 120$. However, very good history matches are achieved with far fewer basis functions. This is shown in Fig. 13, which depicts the minimum value of Problem 2 that is achieved with $L = 1, \dots, 10$. Note that V decreases by five orders of magnitude using only six basis functions. The corresponding updated permeability estimate, depicted in Fig. 14, only shows a resemblance with the true permeability, depicted in Fig. 4, in the vicinity of the wells in which we can control and observe. Moreover, comparison of Figs. 2 and 5 illustrates that the decay in magnitude of singular values is of a similar nature for both cases, which implies that the number of identifiable basis functions is only weakly related to the degree of heterogeneity.

It is interesting to note that we can construct permeability estimates that appear different but lead to virtually the same input–output behavior and, thereby, history match cost function V. Three such estimates are depicted in Fig. 15. These permeability estimates are constructed by adding linear combinations of columns of $\hat{\mathbf{T}}_{\text{bal},2}$ to the estimate depicted in Fig. 14. The corresponding value of the history match cost function V, originally 1.3×10^{-6}, hardly changes.

Finally, it should be noted that this particular application involves history matching with 200 measurements taken every $\Delta t = 0.013$ s, which is clearly not very realistic—see the signals depicted in Fig. 12. This is
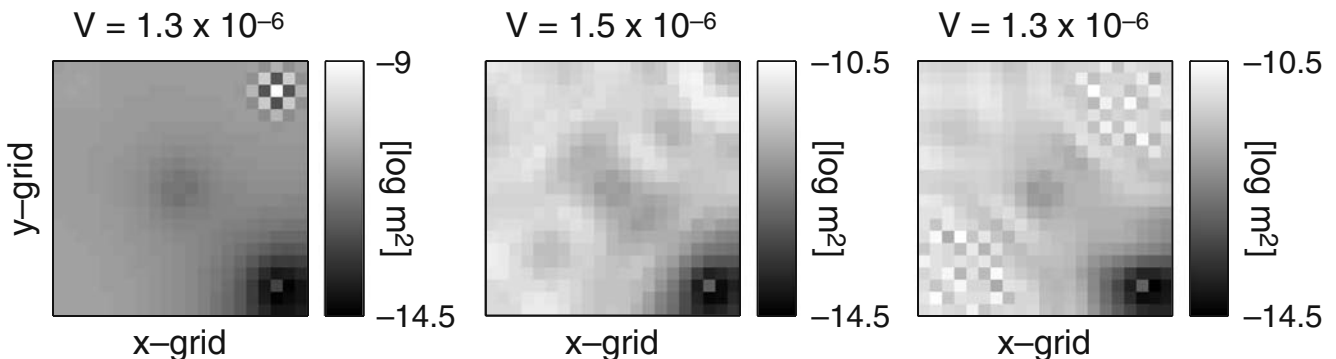

Fig. 15 Alternative estimates of heterogeneous permeability constructed by adding columns of $\hat{\mathbf{T}}_{\text{bal},2}$ to the estimate depicted in Fig. 14, and corresponding values of history match cost function V

due to the reservoir's relatively small size and high permeability, as well as the low compressibility of the fluid. However, for larger reservoirs with lower permeability and higher compressibility, the sampling time Δt can be much larger.

5 Conclusions

The most controllable and observable pressures in single-phase flow reservoir models can be computed by performing an eigenvalue decomposition of the controllability and observability Gramians. By projecting the eigenvectors corresponding to the largest absolute eigenvalues of the Gramians onto the model grid, we can interpret how the reservoir model's controllability and observability properties vary over space. It turns out that pressures near wells in which we can control the flow rate or bottom-hole pressure are controllable, whereas pressures near wells in which we can measure the flow rate or bottom-hole pressure are observable. Furthermore, the controllability and observability properties are determined by the well configuration (i.e., the number and location of wells) and, to a lesser extent, the heterogeneity of the reservoir at hand.

The Hankel singular values of single-phase flow reservoir models decrease rapidly, indicating that they behave as models of much lower order. The latter severely limits the number of identifiable parameters. An upper bound N_{max} for the maximum number of identifiable parameters is given. It is shown that if the vector of to-be-estimated parameters contains the N grid block permeabilities, then $N_{max} \ll N$ and the model structure is not identifiable. Furthermore, by inspecting how the controllable and observable part of a reservoir model depends on permeability, it is shown that the relevant spatial patterns of permeability strongly resemble the relevant spatial patterns of pressure. Consequently, a new method of regularization is to reparameterize permeability through a linear combination of the most relevant spatial patterns of pressure. A history matching example shows that this controllability and observability-based regularization leads to good results.

References

1. Abacioglu, Y., Oliver, D., Reynolds, A.: Efficient reservoir history matching using subspace vectors. Comput. Geosci. **5**, 151–172 (2001)
2. Antoulas, A.C.: Approximation of Large-Scale Dynamical Systems. SIAM, Philadelphia (2005)
3. Astrom, K.J., Wittenmark, B.: Computer Controlled Systems, 2nd edn. Prentice Hall, Englewood Cliffs (1990)
4. Aziz, K., Settari, A.: Petroleum Reservoir Simulation. Applied Science, Barking (1979)
5. Bellman, R., Astrom, K.J.: On structural identifiability. Math. Biosci. **7**, 329–339 (1970)
6. Berre, I., Lien, M., Mannseth, T.: A level-set corrector to an adaptive multiscale permeability prediction. Comput. Geosci. **11**, 27–42 (2007)
7. Bissell, R.C.: Calculating optimal parameters for history matching. In: 4th European Conference on the Mathematics of Oil Recovery, Roros, 7–10 June 1994
8. Bissell, R.C., Sharma, Y., Killough, J.E.: History matching using the method of gradients: two case studies. In: SPE Annual Conference and Exhibition (SPE 28590-MS), New Orleans, 25–28 September 1994
9. Brun, B., Gosselin, O., Barker, J.W.: Use of prior information in gradient-based history matching. SPE J. (SPE 87680-PA) **9**(1), 67–78 (2004)
10. Carter, R.D., Kemp, L.F., Pierce, A.C., Williams, D.L.: Performance matching with constraints. SPE J. (SPE 4260) **14**, 187–196 (1974)
11. Chavent, G.: History matching by use of optimal theory. SPE J. (SPE 4627) **1**, 74–86 (1975)
12. Chen, C.T.: Linear System Theory and Design, 2nd edn. Holt, Rinehart and Winston, New York (1984)
13. Denham, M.J.: Canonical forms for the identification of multiviarable linear systems. IEEE Trans. Automat. Contr. **19**(6), 646–656 (1974)
14. Gavalas, G.R., Shah, P.C., Seinfeld, J.H.: Reservoir history matching by Bayesian estimation. SPE J. (SPE 5740-PA) **16**(6), 337–350 (1976)
15. Gildin, E., Klie, H., Rodriguez, A., Wheeler, M.F.: Development of low-order controllers for high-order reservoir models and smart wells. In: SPE Annual Techical Conference and Exhibition (SPE 102214-MS), San Antonio, 24–27 September 2006
16. Glover, K.: All optimal hankel-norm approximations of linear multivariable systems and their $\mathcal{L}^\infty$-error bounds. Int. J. Control **39**(6), 1115–1193 (1984)
17. Glover, K., Willems, J.C.: Parameterizations of linear dynamical systems: Canonical forms and identifiability. IEEE Trans. Automat. Contr. **19**(6), 640–646 (1974)
18. Grimstad, A., Mannseth, T., Naevdal, G.: Adaptive multiscale permeability estimation. Comput. Geosci. **7**(1), 1–25 (2003)
19. Heijn, T., Markovinovic, R., Jansen, J.D.: Generation of low-order reservoir models using system-theoretical concepts. SPE J. (SPE 88361) **9**(2), 202–218 (2004)
20. Jacquard, P., Jain, C.: Permeability distribution from field pressure data. SPE J. (SPE 1307) **5**, 281–294, (1965)
21. Jafarpour, B., McLaughlin, D.B.: Efficient permeability parameterization with the discrete cosine transform. In: SPE Reservoir Simulation Symposium (SPE 106453), Houston, February 2007
22. Jafarpour, B., McLaughlin, D.B.: History matching with an ensemble Kalman filter and discrete cosine parameterization.

In: SPE Annual Technical Conference and Exhibition (SPE 108761), Anaheim, November 2007

23. Jahns, H.O.: A rapid method for obtaining a two-dimensional reservoir description from well pressure response data. SPE J. (SPE 1473-PA) **6**(4), 315–327 (1966)

24. Kalman, R.E.: Mathematical description of linear dynamical systems. SIAM J. Control **1**(2), 152–192 (1963)

25. Li, R., Reynolds, A.C., Oliver, D.S.: History matching of three-phase flow production data. SPE J. (SPE 87336) **8**(4), 328–340 (2003)

26. Ljung, L.: System Identification—Theory for the User, 2nd edn. Prentice Hall, Englewood Cliffs (1999)

27. Luenberger, D.G.: Canonical forms for linear multivariable systems. IEEE Trans. Automat. Contr. **12**, 290–293 (1967)

28. Markovinovic, R., Geurtsen, E.L., Heijn, T., Jansen, J.D.: Generation of low-order reservoir models using POD, empirical Gramians and subspace identification. In: 8th European Conference on the Mathematics of Oil Recovery, Freiberg, 3–6 September 2002

29. Moore, B.C.: Principal component analysis in linear systems: controllability, observability, and model reduction. IEEE Trans. Automat. Contr. **26**(1), 17–32 (1981)

30. Reynolds, A.C., He, N., Chu, L., Oliver, D.S.: Reparameterization techniques for generating reservoir descriptions conditioned to variograms and well-test pressure data. SPE J. (SPE 30588-PA) **1**(4), 413–426 (1996)

31. Sarma, P., Durlofsky, L.J., Aziz, K., Chen, W.H.: A new approach to automatic history matching using kernel PCA. In: SPE Reservoir Simulation Symposium (SPE 106176), Houston, February 2007

32. Shah, P.C., Gavalas, G.R., Seinfeld, J.H.: Error analysis in history matching: the optimum level of parameterization. SPE J. (SPE 6508-PA) **18**(3), 219–228 (1978)

33. Tarantola, A.: Inverse Problem Theory and Methods for Model Parameter Estimation. SIAM, Philadelphia (2005)

34. Tavassoli, Z., Carter, J.N., King, P.R.: Errors in history matching. SPE J. (SPE 86883) **9**(3), 352–361 (2004)

35. Van Doren, J.F.M., Van den Hof, P.M.J., Jansen, J.D., Bosgra, O.H.: Determining identifiable parameterizations for large-scale physical models in reservoir engineering. In: Proceedings of the 17th IFAC World Congress, Seoul, 6–11 July 2008